Regional Differences in Distribution and Functional Expression of Small-Conductance Ca^{2+}-Activated K^+ Channels in Rat Brain

Claudia A. Sailer,[1] Hua Hu,[3] Walter A. Kaufmann,[1] Maria Trieb,[1] Christoph Schwarzer,[2] Johan F. Storm,[3] and Hans-Günther Knaus[1]

[1]Institute for Biochemical Pharmacology and [2]Institute for Pharmacology, University Innsbruck, A-6020 Innsbruck, Austria, and [3]Institute for Physiology, University of Oslo, N-0317 Oslo, Norway

Small-conductance Ca^{2+}-activated K^+ (SK) channels are important for excitability control and afterhyperpolarizations in vertebrate neurons and have been implicated in regulation of the functional state of the forebrain. We have examined the distribution, functional expression, and subunit composition of SK channels in rat brain. Immunoprecipitation detected solely homotetrameric SK2 and SK3 channels in native tissue and their constitutive association with calmodulin. Immunohistochemistry revealed a restricted distribution of SK1 and SK2 protein with highest densities in subregions of the hippocampus and neocortex. In contrast, SK3 protein was distributed more diffusely in these brain regions and predominantly expressed in phylogenetically older brain regions. Whole-cell recording showed a sharp segregation of apamin-sensitive SK current within the hippocampal formation, in agreement with the SK2 distribution, suggesting that SK2 homotetramers underlie the apamin-sensitive medium afterhyperpolarizations in rat hippocampus.

Key words: SK channels; potassium channels; apamin; antibodies; afterhyperpolarization; subunit composition; distribution

Molecular cloning of small-conductance Ca^{2+}-activated K^+ (SK) channels has revealed three genes, SK1–SK3 (Kohler et al., 1996). When expressed in *Xenopus* oocytes, the resulting channels are voltage-insensitive and activated by submicromolar intracellular Ca^{2+} (Kohler et al., 1996; Hirschberg et al., 1998). Structure–function analysis revealed that their Ca^{2+} gating is mediated by constitutive association with calmodulin (Xia et al., 1998; Keen et al., 1999). However, direct interaction of calmodulin with native brain SK channels so far has been demonstrated only for SK3 (Xia et al., 1998).

In many neurons, action potentials are followed by afterhyperpolarizations (AHPs) consisting of several phases, reflecting the activation of different K^+ currents. Hippocampal pyramidal cells show three different AHPs: fast, medium (mAHP), and slow (sAHP) (Storm, 1987, 1990; Sah, 1996). Because SK2 and SK3 channels are highly apamin-sensitive (picomolar range), they are believed to contribute to the formation of the apamin-sensitive mAHP component and the corresponding current (Sah, 1996; Vergara et al., 1998; Xia et al., 1998; Stocker et al., 1999). For clarity, we will use the term I_{aAHP} for the apamin-sensitive component of the mAHP current, because other current components [muscarin-sensitive K^+ (M)-current, large-conductance Ca^{2+}-activated K^+ (BK)-channel-mediated current, and hyperpolarization-activated cation current] are also known to contribute to the mAHP (Storm, 1989, 1990; Williamson and Alger, 1990). In contrast to SK2 and SK3 channels, homomeric SK1 channels show a significantly lower apamin sensitivity (nanomolar range). It was therefore suggested that the sAHP is mediated by SK1 channels. However, the findings that the sAHP is resistant to apamin (up to 1 μM; Lancaster and Nicoll, 1987; Storm, 1989; Stocker et al., 1999), whereas SK1 homomeric channels are blocked by this toxin (Shah and Haylett, 2000a; Strobaek et al., 2000; Grunnet et al., 2001a), have, together with other pharmacological and kinetic discrepancies, cast doubt on the proposed causal relationship between SK1 and the sAHP (Shah and Haylett, 2000b; Shah et al., 2001; Faber and Sah, 2002). Meanwhile, a complex alternative splicing pattern of mouse and rat SK1 genes have been discovered (Shmukler et al., 2001), with some splice variants lacking the calmodulin-binding domain.

To determine which SK proteins underlie the various ionic currents and AHPs, detailed information regarding the distributions of the SK subunits is required. However, so far our knowledge of these distributions in the brain has been based on *in situ* hybridization data (Kohler et al., 1996; Stocker et al., 1999; Stocker and Pedarzani, 2000) and a few reports using antibodies directed against SK1 and SK3 protein (Bond et al., 2000; Bowden et al., 2001; Tacconi et al., 2001).

In this study, we have used a combination of immunological, pharmacological, and electrophysiological tools to determine the distribution and functional expression of all three SK channel genes in rat brain. These results may help clarify unsolved discrepancies of functional and pharmacological properties of SK channels.

MATERIALS AND METHODS

Materials

[^{125}I]Apamin (2175 Ci/mmol) was obtained from PerkinElmer Life Sciences (Boston, MA), and SuperSignal West dura extended substrate was from Pierce (Rockford, IL). Protein A-Sepharose, sodium cholate, peroxidase-conjugated goat anti-rabbit IgG (used for Western blots), and 3,3′ diaminobenzidine were from Sigma (Munich, Germany). A mono-

Received July 8, 2002; revised Sept. 4, 2002; accepted Sept. 6, 2002.

This work was supported by European Community Grants BMH4-CT97-2118 and QLRT-1999-01356 (J.F.S. and H.-G.K), Austrian Research Foundation Grant P14954-PHA (H.-G.K), the Norwegian Medical Research Council, and the Nansen and Odd Fellow Foundations. This report is part of the PhD theses of C.A.S. and H.H. We thank Dr. Hartmut Glossmann for continuous support. *Xenopus* oocyte membranes were kindly supplied by Dr. Dan Klaerke, Pannum Institute (Copenhagen, Denmark).

Correspondence should be addressed to Hans-Günther Knaus, Institut für Biochemische Pharmakologie, Peter-Mayr Strasse 1, A-6020 Innsbruck, Austria. E-mail: hans.g.knaus@uibk.ac.at.

clonal mouse IgG_1 anti-calmodulin antibody (05-173) was purchased from Upstate Biotechnology (Lake Placid, NY). Horseradish peroxidase-coupled goat anti-rabbit IgG (0448) was purchased from Dako (Glostrup, Denmark). Apamin was bought from Calbiochem (San Diego, CA), and 9-fluorenylmethoxycarbonyl lysine core solid phase support was from NovaBiochem (Laeufelfingen, Switzerland). Cyanogen bromide (CNBr)-activated Sepharose 4B was obtained from Amersham Biosciences (Uppsala, Sweden). The M-channel blocker 10,10-bis-(pyridinylmethyl)-9(10H)-anthracenone (XE991) was obtained from DuPont (Billerica, MA). All remaining drugs were from Sigma. Substances for slice electrophysiology were bath-applied by adding them to the superfusing medium.

Antibody production and affinity purification

Polyclonal sera were raised against SK1 protein (GenBank accession number U69885), residue positions 12–29, using the sequence QPLGSGPGFLGWEPVDPE (anti-$SK1_{(12–29)}$) and 515–532, using the sequence HLTTAAQSPQSHWLPTTA (anti-$SK1_{(515–532)}$); SK2 protein (GenBank accession number U69882), residue position 538–555, using the sequence RDFIETQMENYDKHVTYN (anti-$SK2_{(538–555)}$); and SK3 protein (GenBank accession number U69884), residue position 504–522, using the sequence ADTLRQQQQQLLTAFVEAR (anti-$SK3_{(504–522)}$) (Kohler et al., 1996). Antibodies were raised and affinity-purified as described previously (Knaus et al., 1995).

Immunoblot analysis

Immunoblot analysis was performed as described by Knaus et al. (1995) with some minor modifications. Purified hippocampal synaptic plasma membrane vesicles (10–30 μg/lane) or crude oocyte membranes were separated by 10% SDS-PAGE and transferred to polyvinylidene difluoride (PVDF) membranes. The membrane was blocked with 3% BSA, 0.5% (w/v) Triton X-100, and 0.1% (w/v) Tween 20 dissolved in Tris-buffered saline (TBS) for either 120 min at 22°C or 12–15 hr at 4°C. Thereafter, the blots were incubated with anti-SK antibodies (affinity-purified anti-$SK1_{(12–29)}$, 1 ng/μl IgG; affinity-purified anti-$SK1_{(515–532)}$, 2 ng/μl IgG; and crude serum of anti-$SK2_{(538–555)}$ and anti-$SK3_{(504–522)}$, 1:5000 and 1:13000, respectively) or purified mouse monoclonal anti-calmodulin antibody (Upstate Biotechnology; 1:1000) diluted in 3% BSA, 0.5% Triton X-100, and 0.1% Tween 20 for 12 hr at 4°C. Blots were washed three times with 0.5% Triton X-100 and 0.1% Tween 20 in TBS and incubated with affinity-purified horseradish peroxidase-conjugated goat anti-rabbit or anti-mouse IgG for 120 min at 22°C. After washing six times with the buffer described above, blots were developed using the SuperSignal West dura extended substrate detection kit according to the manufacturer's protocol.

Immunocytochemistry

Immunocytochemical experiments were performed in slight variations to our previous study (Knaus et al., 1996) using free-floating 40 μm cryosections of 4% (w/v) paraformaldehyde-perfused rat brains. Brain sections were permeabilized for 60 min in TBS, pH 7.4, and 0.4% (w/v) Triton X-100, subsequently blocked in 10% normal goat serum (NGS) in TBS and Triton X-100 for 90 min, and incubated overnight in 3% NGS containing affinity-purified anti-$SK1_{(12–29)}$ antibody at a concentration of 2 ng/μl. Crude antiserum of $SK2_{(538–555)}$ was used at final dilutions of 1:4000–1:9000, whereas anti-$SK3_{(504–522)}$ antiserum was diluted 1:12000–1:15000 or used at a concentration of 1.3 ng/μl for affinity-purified antibody. Three rinses in TBS and Triton X-100 were performed before incubation with secondary antibody (horseradish peroxidase-coupled goat anti-rabbit IgG, 1:400) for 150 min. After three washes with TBS, pH 8 (in mM: 20 Tris-HCl, pH 8, and 150 NaCl), antigen-antibody complexes were visualized by reaction with 3,3′-diaminobenzidine, nickel ammonium sulfate, and H_2O_2 in TBS, pH 8, at final concentrations of 0.63 mM, 10 mM, and 0.002%, respectively (Wouterlood, 1988). In control sections, nonspecific immunoreactivity was assessed by preadsorbing primary antibodies with a 10 μM concentration of the respective peptide, incubations without the primary antibody, or using preimmune serum (see Fig. 3). After immunostaining, the preparations were dehydrated in an ethanol series, cleared with butylacetate, and mounted in EuKitt (Christine Groepl, Vienna, Austria). The sections were analyzed using a Zeiss (Oberkochen, Germany) Axioplan 2 microscope equipped with a Zeiss Axio Cam digital camera.

Preparation of purified synaptic plasma membrane vesicles from rat whole brain or hippocampus

Rats (Sprague Dawley, 150–250 gm) were killed by CO_2 inhalation and decapitated; their brains were rapidly removed; the hippocampus was dissected; and the tissue placed in ice-cold homogenization media (320 mM sucrose, 10 mM Tris-HCl, pH 7.4, 1 mM K_2-EDTA, 10 μM PMSF, 10 μM benzamidine, and 1 μM pepstatin A). Synaptic plasma membrane vesicles were prepared by fractionated centrifugation of homogenated brain tissue followed by 7.5/10.0% Ficoll gradient centrifugation (to isolate intact synaptosomes) (Lai et al., 1977). Synaptosomes were lysed, and the respective plasma membrane fraction was isolated by sucrose density gradient centrifugation (Vazquez et al., 1990). Plasma membrane enrichment through the different preparation steps was monitored using radioligand binding for established plasma membrane marker proteins (e.g., [^{3}H]isradipine for L-type Ca^{2+} channels, [^{125}I]ω-conotoxin GVIA for N-type Ca^{2+} channels, [^{125}I]iberiotoxin for high-conductance Ca^{2+}-activated K^+ channels, and [^{125}I]apamin for small-conductance Ca^{2+}-activated K^+ channels). On average, specific activity of the final membrane preparation was enriched 8- to 12-fold compared with the respective starting material (data not shown).

Preparation of Xenopus *oocyte membranes expressing SK channels*

For membrane preparation, batches of 60–80 oocytes injected with SK1, SK2, or SK3 (Kohler et al., 1996) or noninjected oocytes were homogenized in 10% sucrose dissolved in homogenization buffer [600 mM KCl, 5 mM 3-(*N*-morpholino)propanesulfonic acid (MOPS), 100 μM PMSF, 1 μM pepstatin A, 1 μM *p*-aminobenzamide, 1 μg/ml aprotinin, and 1 μg/ml leupeptin, pH 6.8] in a volume of 10 μl/oocyte with 10 strokes at 1000 rpm in a glass–Teflon homogenizer (Braun-Melsungen) at 0°C. The homogenate was placed on top of a step gradient consisting of 7 ml of 50% sucrose and 3.5 ml of 20% sucrose in homogenization buffer and centrifuged at 67,000 × *g* for 30 min at 4°C in a Beckman SW 40 rotor. The interface (between 20 and 50% sucrose) was collected and subjected to centrifugation at 84,000 × *g* for 30 min at 4°C in a Beckman Ti 70.1 rotor. The supernatant was discarded, and the pellet was resuspended in 200 μl of (in mM): 300 sucrose, 100 KCl, and 5 MOPS, pH 6.8, and stored at −80°C until use.

Solubilization of rat brain SK channels, immunoprecipitation studies, and in vitro *[^{125}I]apamin binding studies*

Solubilization. Rat brain synaptic plasma membrane vesicles were sedimented (45,000 × *g*, 15 min), and the resulting pellet was resuspended in (in mM): 5 Tris-HCl, pH 7.4, 0.1 PMSF, 1 iodoacetamide, and 0.1 benzamidine containing 4% (w/v) sodium cholate and 500 mM KCl at a final protein concentration of 20 mg/ml. After incubation, with intermittent mixing, at 1°C for 60 min, insoluble material was sedimented at 106,000 × *g* for 60 min.

Immunoprecipitation and in vitro *[^{125}I]apamin binding studies.* For all experiments, crude anti-$SK1_{(12–29)}$, anti-$SK1_{(515–532)}$, anti-$SK2_{(538–555)}$, and anti-$SK3_{(504–522)}$ serum or a combination thereof was prebound to an equal amount of packed protein A-Sepharose in radioimmunoassay (RIA) buffer (5 mM Tris-HCl, pH 7.4, 5 mM KCl, 0.1% BSA, and 0.3% sodium cholate) for 60–120 min under gentle rotation. The gel was washed three times with 1 ml of RIA buffer before the addition of sodium cholate-solubilized SK channels. The solubilized material was diluted twofold in RIA buffer to lower the detergent and KCl concentration and added to the prebound antibodies, and incubation was continued for 12 hr at 4°C. Each protein A-Sepharose pellet was split into six equal samples, and antibody-bound SK channels were determined by [^{125}I]apamin binding (three samples for control binding and three samples for nonspecific binding). The incubation medium (200 μl) consisted of RIA buffer. Nonspecific binding was defined in the presence of 30 nM apamin, and incubation was performed at 4°C. After 60 min of incubation with the radioligand in the absence (control) or presence of apamin (nonspecific binding), the protein A-Sepharose was rapidly washed three times with ice-cold RIA buffer, and bound [^{125}I]apamin was determined by gamma radiation counting. Under these conditions, a saturating concentration of anti-$SK2_{(538–555)}$ (e.g., 25 μl of serum) typically precipitated 11000–25000 cpm of [^{125}I]apamin (<200 cpm in the presence of 30 nM apamin), whereas the respective preimmune serum precipitated <350 cpm of [^{125}I]apamin (<200 cpm in the presence of 30 nM apamin).

Coimmunoprecipitation and cross-blotting. Anti-$SK2_{(538–555)}$ and anti-$SK3_{(504–522)}$ antibodies were affinity-purified as described previously

(Knaus et al., 1995) and subsequently coupled to CNBr-activated Sepharose 4B according to the manufacturer's protocol. Solubilized material was diluted threefold in (in mM): 5 Tris-HCl, pH 7.4, and 150 NaCl buffer and incubated with the respective antibody column for 36 hr at 4°C. Columns were washed with 40 bed volumes of 0.1% Triton in (in mM): 5 Tris-HCl, pH 7.4, and 150 NaCl. Retained SK2 and SK3 channels were eluted with 0.1 M glycine, pH 2.5, 0.1% Triton X-100, and 150 mM NaCl. IgG leaching from the antibody column was diminished by addition of protein A-Sepharose to the eluted material for 1 hr at 20°C. Eluates were separated by SDS-PAGE and Western blotting was performed as described above.

Slice electrophysiology

Slice preparation. Young male Wistar rats (17–35 d) were deeply anesthetized with halothane before decapitation. Transverse hippocampal slices (400 μm thick) were prepared using a Vibratome (752M; Campden Instruments, Loughsborough, UK) and maintained in artificial CSF (ACSF) containing (in mM): 125 NaCl, 25 $NaHCO_3$, 1.25 KCl, 1.25 KH_2PO_4, 1.5 $MgCl_2$, 1 $CaCl_2$, and 16 glucose and saturated with 95% O_2 and 5% CO_2.

Whole-cell recording and drug application. During recording, the slices were kept at room temperature and superfused with ACSF of the above composition, except that the concentration of $CaCl_2$ was raised to 2 mM. Whole-cell gigaohm seal recordings were obtained from CA1 pyramidal cells using the "blind" method. The patch pipettes were filled with a solution containing (in mM): 140 K-gluconate, 10 HEPES, 2 ATP Na salt, 0.4 GTP Na salt, and 2 $MgCl_2$, resulting in a pipette resistance of 4–7 MΩ. The cells were voltage-clamped using an Axopatch 1D amplifier (Axon Instruments, Foster City, CA), and signals were filtered at 2 kHz (−3 dB). The series resistance was 10–26 MΩ, and all potentials were corrected for the liquid junction potential (−10 mV). To record the SK channel-mediated K^+ currents in relative isolation, tetrodotoxin (TTX, 1 μM) and tetraethylammonium (TEA, 5 mM) were routinely added to the extracellular medium to block Na^+ channels and BK, M, and delayed rectifier K^+ channels. SK channels are known to be relatively insensitive to TEA. Thus, Ishii et al. (1997) found that 5 mM TEA blocks only ~25% of the current through SK1 homomeric channels expressed in *Xenopus* oocytes.

In some experiments, the selective M-channel blocker XE991 (10 μM) was added to the extracellular medium in addition to 5 mM TEA to block any remaining M-current. However, XE991 had no apparent additional effects, indicating that the M-current was already fully blocked by 5 mM TEA (Storm, 1989, 1990). The whole cell capacitance (C_m) was calculated according to the formula $C_m = (\int dI/dt)/V$; where V is the amplitude of a negative voltage-clamp step (−10 mV, 10 msec long) and $\int dI/dt$ is the time integral of the capacitative current transient after the end of the negative step.

Data acquisition, storage, and analysis

The data were acquired using pClamp 7.0 (Axon Instruments) at a sampling rate of 1 kHz, digitized (10 kHz), stored on videotapes (Instrutec VR-10), analyzed, and plotted using pClamp 7.0 and Origin 5.0 (Microcal). The peak of the mAHP current (I_{mAHP}) was measured by averaging the amplitude measurements within a 10 msec time window 50 msec after the end of depolarizing step; this time window always corresponded to the peak of I_{mAHP}. Because the time to peak was more variable for the sAHP current (I_{sAHP}), we used a different method to measure its amplitude. The current trace within a time window that included I_{sAHP} but excluded I_{mAHP} was low-pass-filtered at 100 Hz to reduce the high-frequency noise, and the peak amplitude was determined at the time point at which the filtered I_{sAHP} was maximal.

Values are expressed as mean ± SEM. Two-tailed paired Student's t test was used for statistical analysis ($\alpha = 0.05$).

RESULTS

Characterization of SK-specific antibodies in immunoblot analysis of rat brain

Anti-$SK1_{(12–29)}$, anti-$SK1_{(515–532)}$, anti-$SK2_{(538–555)}$, and anti-$SK3_{(504–522)}$ sequence-directed antibodies against the pore-forming subunits of SK1, SK2, and SK3 channels were applied to investigate the presence and apparent molecular weight of their tissue-expressed gene products. All antibodies specifically recognized both the respective *in vitro*-translated SK channels (data not shown) and SK1, SK2, or SK3 protein after expression in *Xenopus* oocytes followed by isolation of the plasma membrane fraction (Fig. 1). In *Xenopus* oocytes, the respective SK antibodies recognized immunoreactive bands of 69 kDa (SK1), 64 kDa (SK2), and 67 kDa (SK3).

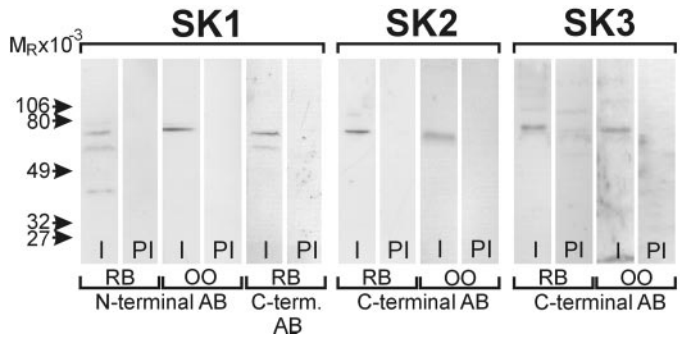

Figure 1. Immunological identification of SK channel protein in rat hippocampus and *Xenopus* oocyte membranes: characterization of anti-SK antibodies in Western blotting experiments. Twenty micrograms of purified rat hippocampal synaptic plasma membrane vesicles or *Xenopus* oocyte membranes expressing SK1, SK2, or SK3 channels were separated by 10% SDS-PAGE and transferred to PVDF membranes. SK proteins were detected by the respective antibodies following standard procedures. SK1 protein, 65, 58, and 43 kDa in rat brain and 69 kDa in oocyte membranes (*N-terminal AB*); SK1 protein, 65 and 58 kDa in rat brain membranes (*C-terminal AB*); SK2 protein, 67 kDa in rat brain and 64 kDa in oocyte membranes; SK3 protein 70 kDa in rat brain and 67 kDa in oocyte membranes. *AB*, Antibody; *I*, immune serum; *PI*, preimmune serum; *RB*, rat brain membranes; *OO*, oocyte membranes;

In purified synaptic plasma membrane vesicles from rat whole brain, anti-$SK1_{(12–29)}$ stained three diffuse bands with apparent M_r values of 65, 58, and 43 kDa, whereas the respective C-terminal antibody anti-$SK1_{(515–532)}$ exclusively stained polypeptides with apparent M_r values of 65 and 58 kDa. An identical polypeptide pattern was observed for mouse whole-brain membranes (data not shown). In contrast, anti-$SK2_{(538–555)}$, and anti-$SK3_{(504–522)}$ stained single bands with overall M_r values of 67 and 70 kDa, respectively (Fig. 1). The observed M_r values for SK2 and SK3 channels are in good agreement with the deduced M_r values (SK2, 64 kDa; SK3, 63 kDa; for considerations regarding the polypeptides detected by anti-$SK1_{(12–29)}$ and anti-$SK1_{(515–532)}$, see Discussion). The immunostaining signal was substantially reduced by inclusion of 10 μM immunogenic peptide (data not shown) and not present when using the respective preimmune sera (Fig. 1).

Subunit composition of apamin-sensitive SK channels in rat brain

To investigate further the molecular components of SK channels in rat brain, these channels were solubilized with sodium cholate; the individual channel population was immunoprecipitated by the corresponding antibodies; and the amount of channel precipitated was quantified by [^{125}I]apamin binding. In all cases, the respective preimmune sera precipitated <5% compared with the corresponding immune sera (Fig. 2*B*). Although anti-$SK2_{(538–555)}$ and anti-$SK3_{(504–522)}$ yielded saturable levels of [^{125}I]apamin-binding precipitation, both anti-$SK1_{(12–29)}$ and anti-$SK1_{(515–532)}$ failed to immunoprecipitate [^{125}I]apamin binding to a significant extent (Fig. 2*A*). Anti-$SK2_{(538–555)}$ precipitated 71 ± 5% ($n = 3$) of soluble apamin receptors, whereas anti-$SK3_{(504–522)}$ precipitated 29 ± 7% ($n = 3$) of the sites. However, the combination of both antisera resulted in strict additivity, indicating complete segrega-

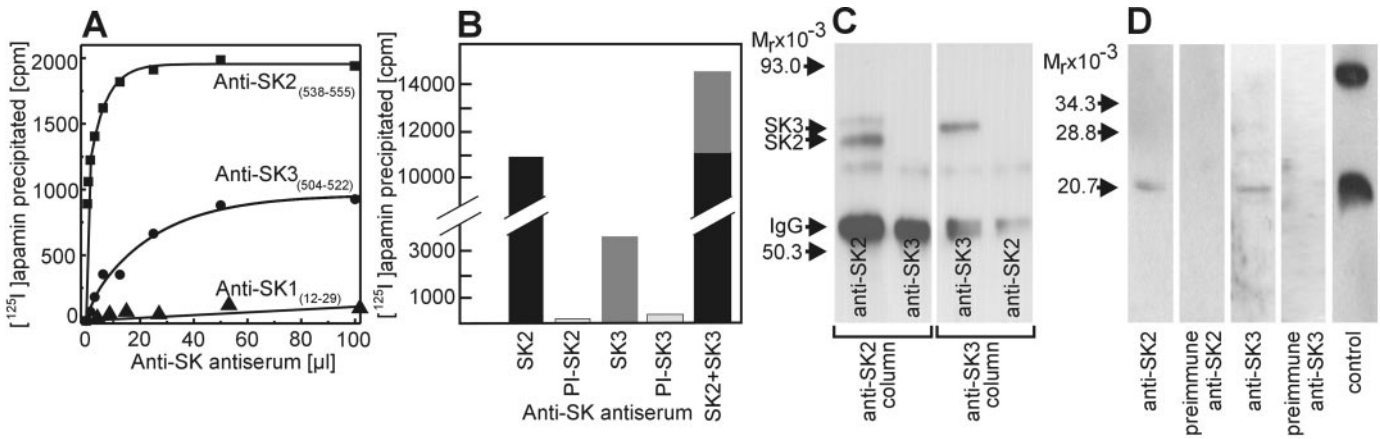

Figure 2. Immunoprecipitation of detergent-solubilized SK channel complexes. *A*, Cholate-solubilized SK channels were immunoprecipitated using increasing concentrations of anti-$SK1_{(12–29)}$ (▲), anti-$SK2_{(538–555)}$ (■), or anti-$SK3_{(504–522)}$ (●) antibodies immobilized on protein A-Sepharose. Immunoprecipitated channels were quantified by [^{125}I]apamin binding to antibody-bound SK channels. In this experiment, anti-$SK2_{(538–555)}$ saturably precipitated 2100 cpm, whereas anti-$SK3_{(504–522)}$ immobilized 930 cpm. Anti-$SK1_{(12–29)}$ was unable to precipitate any [^{125}I]apamin binding. One representative experiment is shown. *PI*, Preimmune serum. *B*, Cholate-solubilized neuronal SK channels were immunoprecipitated by a saturating amount of anti-$SK2_{(538–555)}$ and anti-$SK3_{(504–522)}$ antibodies or a combination thereof. The extent of immunoprecipitation was quantified by [^{125}I]apamin binding to antibody-immobilized SK channels. Exclusively anti-$SK2_{(538–555)}$ and anti-$SK3_{(504–522)}$ antibodies were capable of immunoprecipitating [^{125}I]apamin binding, whereas the corresponding preimmune sera did not immobilize soluble apamin-sensitive SK channels. *C*, Solubilized neuronal SK channels were immunoaffinity-purified by column chromatography using anti-$SK2_{(538–555)}$ or anti-$SK3_{(504–522)}$. Eluates were analyzed by Western blotting using anti-SK antibodies as indicated. Note that the SK3 antibody does not recognize anti-SK2-immunoprecipitated material and vice versa. *D*, Immunoblot analysis of anti-$SK2_{(538–555)}$- and anti-$SK3_{(504–522)}$-immunoprecipitated material for the presence of calmodulin. Equal amounts of detergent-solubilized material were subjected to immunoprecipitation. Immunoreactivity observed in the *control lane* corresponds to monomeric and dimeric calmodulin.

tion of SK2 and SK3 channels into individual channel populations (Fig. 2*B*). Western blot analysis of the remaining supernatant indicated complete clearance from soluble apamin-sensitive SK channels (data not shown). Additional support stems from cross-blotting experiments using anti-$SK2_{(538–555)}$ and anti-$SK3_{(504–522)}$ immunoaffinity columns (Fig. 2*C*). Although anti-$SK2_{(538–555)}$ is clearly capable of retaining SK2 channels, this antibody failed to coimmunoprecipitate SK3 channels. In support of these data, anti-$SK3_{(504–522)}$ immunoaffinity purified solely SK3 channels; however, no SK2 channels were detected through this cross-blotting approach.

Because [^{125}I]apamin failed to detect SK1 channels being precipitated by the respective antibodies, this cross-blotting approach was also attempted. However, neither of the anti-SK antibodies was capable of immunoprecipitating detergent-solubilized SK1 protein. This finding indicates that none of our anti-SK1 antibodies is suitable for immunoprecipitation experiments; therefore, no conclusion regarding subunit composition or association of SK1 channels with calmodulin can be drawn.

After providing evidence that SK2 and SK3 subunits do not coassemble to form heterotetrameric SK2/SK3 channels, we next investigated whether calmodulin is constitutively bound to rat brain SK channels. As shown in Figure 2*D*, both anti-$SK2_{(538–555)}$ and anti-$SK3_{(504–522)}$ coimmunoprecipitated calmodulin. This precipitation was specific, because a corresponding amount of the respective preimmune serum failed to precipitate calmodulin. The result with the anti-SK3 antibody is in good agreement with a previous report (Xia et al., 1998).

Regional distribution of SK protein in neocortex and hippocampal formation

Specificity of immunostaining

The neuronal distribution pattern of all three subunits was investigated by immunohistochemical analysis (Figs. 3, 4). The characteristic immunostaining pattern fulfilled the specificity criteria, because it was not observed with the corresponding preimmune sera (Fig. 3) or in the presence of excess immunogenic peptide (data not shown). It is beyond the scope of this paper to provide a detailed description of the distribution of SK1-, SK2-, and SK3-IR in all brain regions. However, the salient features of the immunohistochemical staining patterns of these three proteins are described below.

Expression of SK1 protein

To obtain a distribution profile of all SK1 proteins independently of alternate splicing, the anti-$SK1_{(12–29)}$ antibody was used for all distribution studies. In the neocortex, almost all SK1 IR was restricted to fibers extending from layer V to layer I (Fig. 4*A*). The staining appeared to be associated with both the proximal and distal dendrites of the layer V pyramidal cells. Little or no IR could be observed in perikarya in this brain region.

However, the highest levels of SK1 protein were expressed in the hippocampal formation, again showing staining associated with the neuropil (Fig. 4*D,G,J*). Virtually no immunostaining was associated with granule and pyramidal cell somata. The molecular layer (inner, middle, and outer parts) of the dentate gyrus, containing the dendrites of granule, basket, and polymorphic cells as well as perforant path terminals, revealed the most prominent staining (Fig. 4*J*). Dense IR could also be observed within the mossy fiber system, with highest levels in the stratum lucidum of the CA3 area. This layer contains three principal structures: pyramidal cell dendrites, mossy fiber axons, and synaptic complexes. Somewhat lower concentrations of the SK1 protein could be detected in stratum oriens and stratum radiatum (Fig. 4*D*). These regions contain, for example, the dendrites of the pyramidal cells as well as the Schaffer collaterals. Interestingly, the signal was slightly discontinuous at the junction between the CA1 and CA3 regions, with a somewhat higher density of IR in CA1 (Fig. 4*G*).

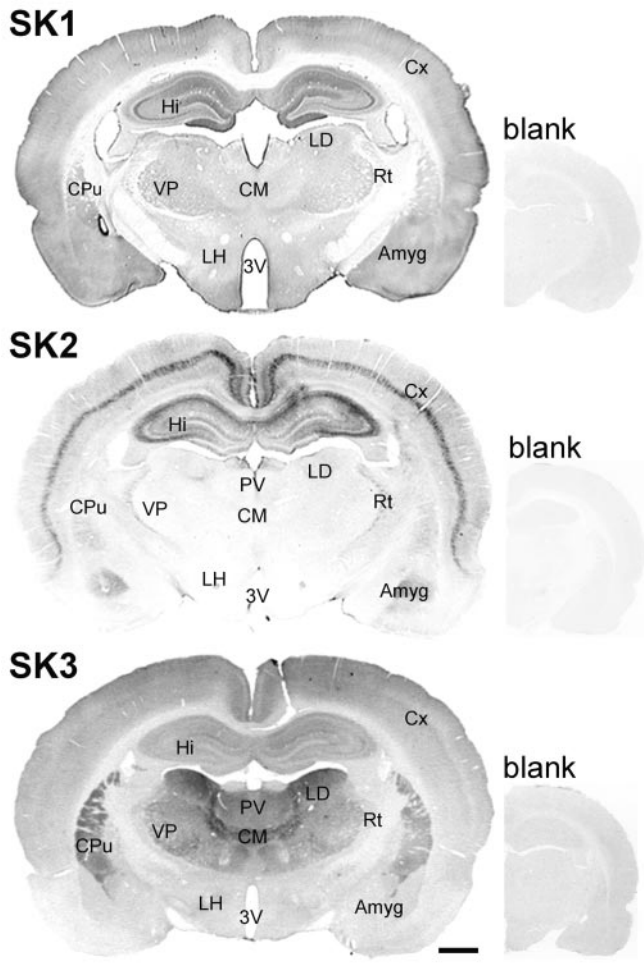

Figure 3. Coronal sections showing the distribution of SK1–SK3 protein in rat brain. Low-magnification microphotographs show the overall distribution of SK1–SK3 immunoreactivity in coronal brain sections. Adjacent sections (40 μm) were stained with affinity-purified anti-SK1$_{(12–29)}$ (2.0 ng/μl IgG), anti-SK2$_{(538–555)}$ 1:6000 (crude serum), and anti-SK3$_{(504–522)}$ (1.3 ng/μl IgG). Nonspecific immunostaining was assessed using preimmune serum. Immune serum preadsorbed to immunogenic peptide yielded essentially identical results. *3V*, Third ventricle; *Amyg*, amygdala, *CM*, centromedial thalamic nucleus; *CPu*, caudate putamen; *Cx*, neocortex; *Hi*, hippocampus; *LD*, laterodorsal thalamic nucleus; *LH*, lateral hypothalamic area; *PV*, paraventricular thalamic nucleus; *Rt*, reticular thalamic nucleus; *VP*, ventroparietal thalamic nucleus. Scale bar, 1000 μm.

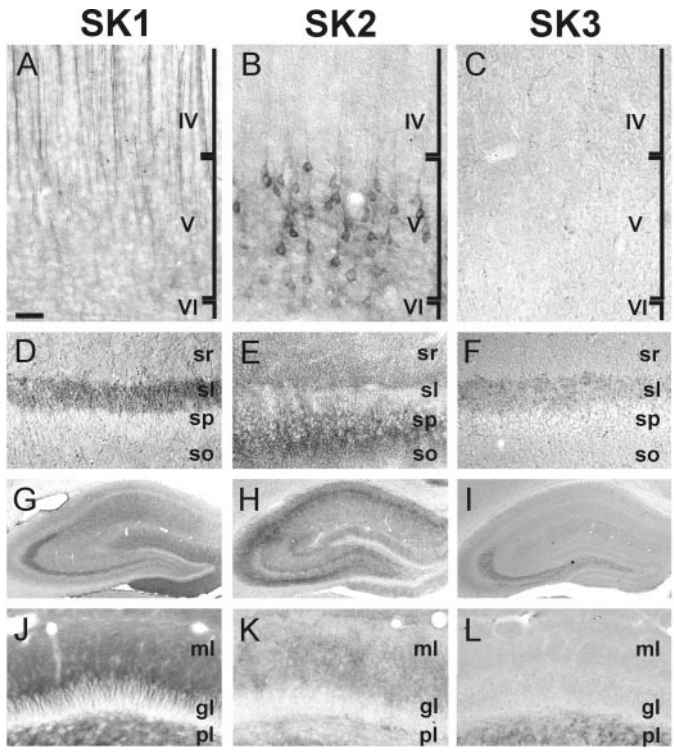

Figure 4. Differential distribution of SK1–SK3 protein in sections of the rat brain: expression of SK proteins in subsets of neurons. *A–C*, SK1–SK3-IR in layers IV–VI of the frontoparietal cortex (coronal brain section). *D–F*, SK1–SK3 localization in the CA3 region of the hippocampus. *G–I*, Localization of SK1–SK3 protein within the hippocampus proper. *J–L*, Distribution of SK1–SK3 protein within the dentate gyrus. *gl*, Granule cell layer; *ml*, molecular layer; *pl*, polymorphic layer; *sl*, stratum lucidum; *sp*, stratum pyramidale; *so*, stratum oriens; *sr*, stratum radiatum. Scale bar: *A–C*, 45 μm; *D–F, J–L*, 100 μm; *G–I*, 400 μm.

Expression of SK2 protein

SK2-IR in the neocortex could be predominantly observed in pyramidal cells of layer V. Distinct staining was associated with the soma as well as with the proximal portion of the dendritic tree (Fig. 4*B*). All other neocortical compartments appeared to be almost devoid of SK2-IR.

In the hippocampal formation, SK2-IR was mainly enriched in the CA1–CA3 region (hippocampus proper) but predominately spared the dentate gyrus (Fig. 4*H*). Within the hippocampus proper, the highest level of SK2 protein was present in the stratum oriens (especially in the layer of the proximal dendrites of pyramidal cells), whereas the strata radiatum and pyramidale showed intermediate to low levels of immunoreactivity, respectively. No SK2 immunostaining was associated with the stratum lucidum of CA3 (Fig. 4*E*). As mentioned before, the dentate gyrus (DG) revealed only low levels of SK2 protein. Faint staining could be observed in the molecular layer, whereas the DG granule cell layer was virtually devoid of SK2-IR (Fig. 4*K*).

Additionally, a limited number of hippocampal interneurons were found to expose SK2-IR. Most of these were found in the stratum oriens, although scattered neurons could be observed throughout the hippocampus.

Expression of SK3 protein

In contrast to SK1 and SK2 protein, the anti-SK3$_{(504–522)}$ antibody revealed only faint staining throughout the entire neocortex. No particular enrichment in any layer could be observed. The most prominent feature was the staining of varicose fibers in all neocortical layers (Fig. 4*C*).

The hippocampal formation showed moderate levels of SK3-IR compared with its expression in the basal ganglia or thalamus. SK3-IR was almost uniformly distributed throughout this brain region but with distinct fiber staining within the hilus and the terminal field of mossy fibers (Fig. 4*I,L*). This suggests an axonal or presynaptic localization of SK3 protein for areas that were mostly devoid of SK2 protein. Virtually no IR could be found for the DG granule cell layer and the superficial molecular layer (Fig. 4*L*). Moderate levels of SK3-IR were also associated with the stratum lacunosum moleculare, a layer in which the perforant path fibers from the entorhinal cortex terminate. A low level of immunostaining was present in the strata oriens and radiatum of CA1–CA3, whereas no IR could be detected in the pyramidal cell layer (Fig. 4*F,I*).

Taken together, the staining patterns of SK1 and SK2 protein were found to be distinct; however, they overlapped in some brain regions. SK3 protein was distributed mostly reciprocally without any significant extent of overlap to SK1 and SK2.

Functional expression of SK channels in rat brain

Given the prominent expression of SK1–SK3 protein in the rat hippocampal formation, we focused our electrophysiological experiments on this brain region.

Whole-cell somatic recordings were obtained from CA1 and CA3 pyramidal cells and granule cells of the dentate gyrus in rat hippocampal slices. To compare the Ca^{2+}-activated K^+ currents (AHP currents; Pennefather et al., 1985; Lancaster and Adams, 1986; Storm, 1990; Stocker et al., 1999) in the three cell populations, each cell was voltage-clamped at a holding potential of −50 or −55 mV. One micromolar TTX and 5 mM TEA were routinely added to the extracellular medium to record the SK currents in relative isolation (see Materials and Methods).

Calcium-activated tail currents were elicited by a brief (100 msec) depolarizing voltage step, which reliably triggered Ca^{2+} influx in the form of an unclamped Ca^{2+} action current (see Materials and Methods; Pedarzani and Storm, 1993). In the CA1 and CA3 pyramidal cells, each depolarizing step was followed by a biphasic outward tail current (AHP currents) consisting of early and late components (Fig. 5*A*). The early outward tail current contributes to the mAHP (Storm, 1989; Stocker et al., 1999), whereas the slow component, lasting 4–7 sec, is called the I_{sAHP} because it underlies the slow AHP (Hotson and Prince, 1980; Lancaster and Adams, 1986; Storm, 1990; Sah, 1996). Both I_{sAHP} and the apamin-sensitive component of the mAHP current were largely resistant to 5 mM TEA but were readily suppressed by perfusion with Ca^{2+}-free medium and by the Ca^{2+} channel blockers Mn^{2+} and Cd^{2+} (data not shown; Lancaster and Adams, 1986; Pedarzani and Storm, 1993; Stocker et al., 1999).

Figure 5 shows typical AHP currents recorded in a CA1 pyramidal cell (Fig. 5*A*), a CA3 pyramidal cell (Fig. 5*B*), and a DG granule cell (Fig. 5*C*). The CA1 and CA3 pyramidal cells showed a large mAHP current followed by a smaller sAHP current. In contrast, the DG cells showed little or no distinct early (mAHP) current, although the I_{sAHP} amplitude was similar to that of CA1 and CA3 pyramidal cells (Fig. 5C). Furthermore, whereas bath application of 100 nM apamin blocked the large mAHP current in both the CA1 and CA3 pyramidal cells, this toxin had only a small effect on the early tail currents of the DG granule cells (Fig. 5*C*). This indicates that the apamin-sensitive SK current is substantially smaller in the latter cell type. In contrast, the sAHP current was relatively similar both in amplitude and time course in the three cell types (Fig. 5, Table 1). Apamin (10 μM) had no measurable effect on I_{sAHP} in any of the three cell types (Fig. 5*A–C*), indicating that this current is generated by apamin-resistant channels (Lancaster and Nicoll, 1987; Storm, 1989).

In the CA3 cells, apamin unmasked an inward tail current (Fig. 5*B*). The nature of this current was not determined in our study, but it is likely to be a Ca^{2+} or Na^+ current, possibly through Ca^{2+}-activated nonselective cation channels (Partridge and Swandulla, 1993). A similar inward tail current that was observed in the DG cells after blocking other K^+ currents was constant throughout the recordings and apparently not affected by apamin (see below). It therefore seems unlikely that our I_{aAHP} measurements were significantly confounded by the inward tail current.

To study the apamin-sensitive current, I_{aAHP}, in relative isolation, we performed the remaining experiments under conditions

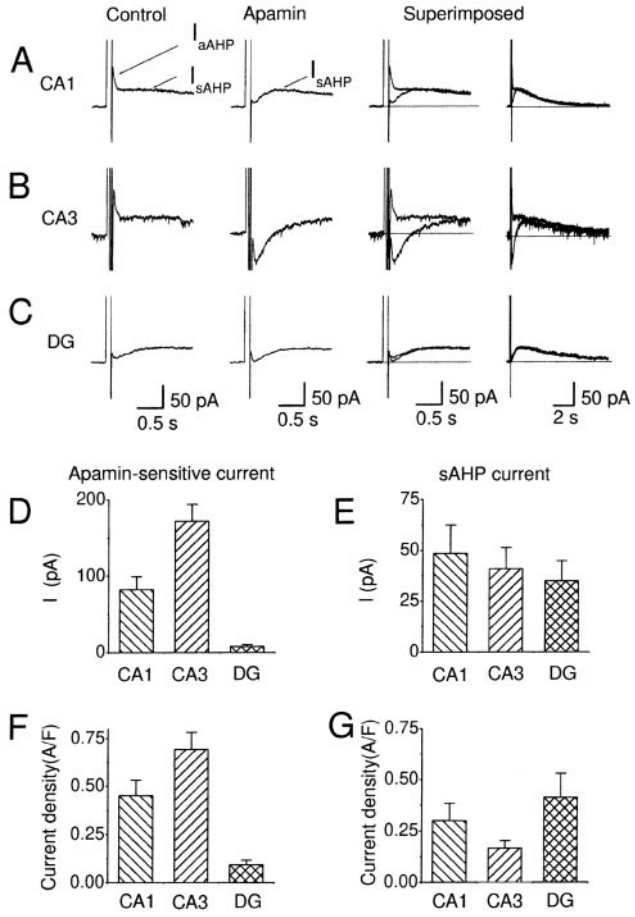

Figure 5. Apamin-sensitive and -insensitive AHP currents in hippocampal pyramidal cells and DG cells. Typical AHP currents recorded in a CA1 pyramidal cell (*A*), a CA3 pyramidal cell (*B*), and a DG granule cell (*C*) in rat hippocampal slices are shown. Each cell was voltage-clamped at –55 mV in the presence of TTX and TEA in the extracellular medium to suppress the Na^+- and BK-channel-mediated currents. The AHP currents were elicited by a brief depolarizing voltage step (100 msec to 0 mV) once every 60 sec. The depolarizing step elicited biphasic outward tail currents in all three cell types (*Control*): an early tail current of medium duration was followed by an I_{sAHP} lasting several seconds. The early current was much larger in CA1 and CA3 pyramidal cells than in DG granule cells. Bath application of 100 nM apamin abolished the early outward tail current in the CA1 and CA3 pyramidal cells but had little or no effect in the DG cells. The records before and after apamin application are compared (*Superimposed*) at two different time scales to show the time course of both components. (The current records in the CA3 cell appeared "noisy" because of a large number of spontaneous miniature synaptic currents.) *D–G*, Summary data comparing currents in CA1 pyramidal cells ($n = 6$), CA3 pyramidal cells ($n = 9$), and DG granule cells ($n = 6$). *D*, Peak amplitudes of the apamin-sensitive tail current obtained by digital subtraction of records taken before and after application of 100 nM apamin. The current was measured 50–60 msec after the end of the depolarizing step. *E*, Peak amplitudes of the apamin-insensitive sAHP current. *F*, *G*, Current densities obtained by dividing the measurements shown in *D* and *E*, respectively, by the whole-cell capacitance measured in each cell. *F*, Current densities for the apamin-sensitive tail current. *G*, Current densities for the apamin-insensitive sAHP current. All currents (*A–G*) were recorded without cAMP in the pipette and in extracellular medium with 1 μM TTX and 5 mM TEA. *D–G*, Mean values and SEM (error bars) for the peak tail currents.

that suppressed I_{sAHP} as well as other K^+ currents (Fig. 6). In these experiments, M-, BK-, and delayed rectifier-type K^+ currents were suppressed by bath application of 10 μM XE991 and 5 mM TEA. In addition, I_{sAHP} was suppressed by inclusion of

Table 1. Cells recorded without cAMP in the pipette

	Apamin-sensitive current, I_{aAHP}				Apamin-insensitive current, I_{sAHP}		
	Amplitude (pA)[a]	Current density (A/F)[a]	Decay time constant (msec)[a,b]	*n*	Amplitude (pA)[a]	Current density (A/F)[a]	*n*
CA1	82.1 ± 16.9	0.45 ± 0.08	225.6 ± 37.6	6	47.1 ± 14.1	0.29 ± 0.08	6
CA3	172.2 ± 21.9	0.69 ± 0.08	365.3 ± 36.3	9	40.8 ± 10.5	0.16 ± 0.04	9
DG	8.2 ± 2.2	0.09 ± 0.02	[c]	6	34.8 ± 9.9	0.41 ± 0.11	6

[a]Values are mean ± SEM.

[b]Fitting with double exponentials was used to give the best fit. The second exponential (not included in the table) had a slow time constant (0.5–5.5 sec) resembling I_{sAHP} and a very small, negative amplitude (−3.3 ± 0.4 pA), suggesting that it reflected a slight indirect enhancement of I_{sAHP} caused by apamin-induced enhanced space clamp resulting in increased Ca^{2+} influx.

[c]The amplitude of the current in DG cells was too small to reliably determine the decay time constant.

cAMP analogues [in μM: 100 cAMP or 100 8 chlorophenylthio (CPT)-cAMP] in the intracellular medium in the recording pipette (Madison and Nicoll, 1986). The SK channels are known to be predominately resistant to these drug concentrations (Ishii et al., 1997; Wang et al., 1998; Hu et al., 2001), but evidence for a small cAMP-induced increase of I_{aAHP} has been reported (Stocker and Pedarzani, 2000). The blockade of non-SK K^+ channels also served to increase the cell input resistance, thereby facilitating the activation of voltage-gated Ca^{2+} channels and, hence, Ca^{2+} influx and SK channel activation and improving the space clamp of the cell. Figure 6 shows representative AHP currents from CA1 (Fig. 6*A*), CA3 (Fig. 6*B*), and DG (Fig. 6*C*) neurons under these conditions.

In response to the same voltage-clamp protocol as used in Figure 5, the CA1 and CA3 pyramidal cells still showed an outward mAHP current, whereas the DG cells showed only an inward tail current under these conditions. Application of apamin again suppressed virtually all mAHP current in CA1 ($n = 9$) and CA3 ($n = 8$) pyramidal cells but had only a small effect in the DG granule cells. Furthermore, 100–600 μM D-tubocurare applied in addition to 100 nM apamin produced no further effect ($n = 20$), suggesting that 100 nM is a saturating concentration of apamin under these conditions (Kohler et al., 1996; Stocker et al., 1999). To isolate the apamin-sensitive current, records taken after the toxin application were digitally subtracted from the control records obtained just before the application (Fig. 6*A–C*, *right traces*). The amplitude of the difference current, I_{aAHP}, was 130–150 pA in the CA1 and CA3 pyramidal cells but only ~30 pA in the DG granule cells (Fig. 6*D,E*). In all cases, the difference in I_{aAHP} amplitude between granule and pyramidal cells was highly significant ($p = 0.00006–0.007$; see Table 3).

The apamin-sensitive current was somewhat larger and more slowly decaying in the CA3 than in the CA1 pyramidal cells (Figs. 5, 6*A,B*). Thus, for cells recorded with cAMP, the decay time constant of I_{aAHP} was 177 ± 30 msec in the CA1 ($n = 9$) versus 297 ± 23 msec in CA3 ($n = 8$; $p = 0.008$; Tables 2, 3). A similar difference was also found in cells recorded without cAMP (Table 1). In addition to I_{aAHP}, two of the eight CA3 cells recorded with cAMP also showed a slower apamin-insensitive outward current component, which was not characterized further in this study.

The small size of the apamin-sensitive SK current in the DG granule cells was apparently not attributable to failure of Ca^{2+} influx during the depolarizing step, because DG granule cells showed a clear Ca^{2+} spike during each voltage step (data not shown), as well as a prominent I_{sAHP}, which was also dependent on Ca^{2+} influx (Fig. 5*C*, Table 1) (Haas and Rose, 1987). We observed no apamin-induced changes in the depolarization-induced Ca^{2+} currents that triggered the AHP currents in each of the three cell types (data not shown), indicating that the action of apamin is downstream of the Ca^{2+} influx.

The difference in whole-cell current is probably related to differences in cell size. To relate the current measurements to the surface membrane area, we calculated the membrane capacitance for each cell from capacitative transients evoked by hyperpolarizing voltage steps (see Materials and Methods) and divided the currents by the capacitance. For the I_{aAHP}, the current densities thus obtained in the CA1, CA3, and DG cells were 0.80, 0.75, and 0.38 pA/pF, respectively. Thus, the I_{aAHP} density in the DG granule cells appears to be only approximately half of that in the CA pyramidal cells (Fig. 6*G*). In contrast, the average density of the sAHP current was somewhat larger in the DG granule cells (0.45 ± 0.11 pA/pF) than in the CA1 and CA3 pyramidal cells (0.29 ± 0.08 and 0.16 ± 0.04 pA/pF, respectively), although the difference was not statistically significant in our data (Fig. 5*G*, Tables 1–3).

In conclusion, there seems to be a substantial difference in the size of the apamin-sensitive SK current between the CA1 and CA3 hippocampal pyramidal cells on one hand and the DG granule cells on the other, whereas the apamin-resistant sAHP current shows no such difference. This holds both for the total current per cell and when corrected for cell size (membrane capacitance, reflecting surface area).

DISCUSSION

This report presents the first distribution profile for all SK channel subunits in a mammalian brain. The data indicate distinct, although partly overlapping, distributions for the three SK subunits and suggest that the apamin-sensitive medium afterhyperpolarization of the hippocampal pyramidal cells is mainly attributable to SK2 protein.

To obtain a complete antibody panel for the individual SK channel subunits, we raised a total of 14 sequence-directed anti-SK channel antibodies of which four antibodies were used to perform this study. The difficulties obtaining suitable SK channel antibodies with high selectivity were mostly attributable to the very low expression density of SK channel protein in mammalian brain (based on radioligand binding data using the SK channel ligand [^{125}I]apamin). This toxin labels only 20–40 fmol of binding sites/mg of protein, a density 10 times lower than for BK-channels (as measured by [^{125}I]iberiotoxin binding; Koschak et al., 1997) or only 1% of the density of toxin-sensitive voltage-gated K^+ channels (e.g., measured by [^{125}I]hongotoxin binding; Koschak et al., 1998) in the same membrane preparation.

Additional complications stem from the fact that the rodent

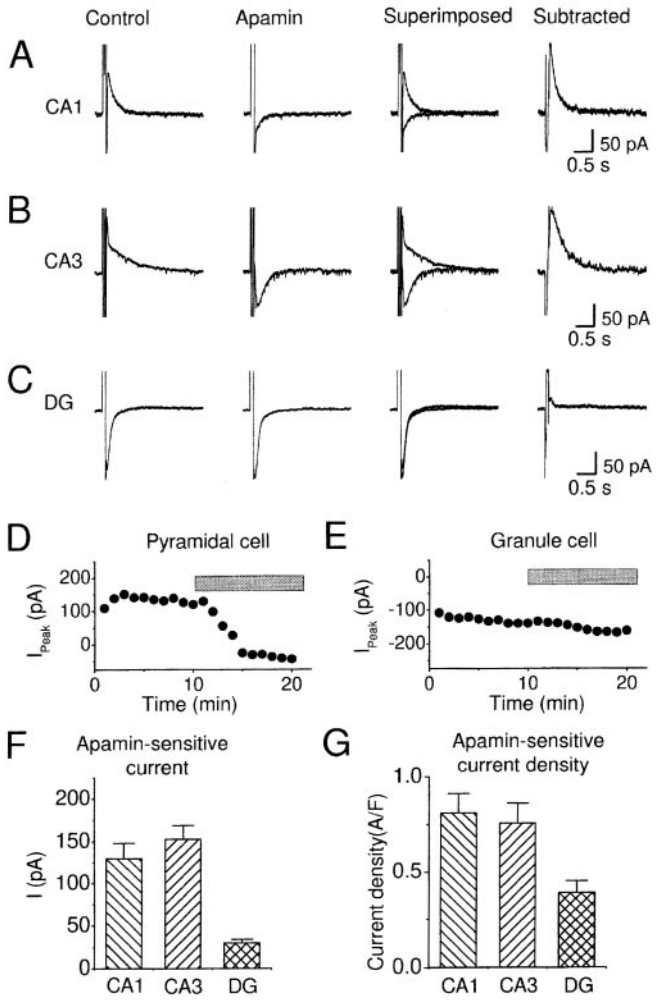

Figure 6. Apamin-sensitive currents in CA1 and CA3 pyramidal cells and DG granule cells recorded after suppression of the sAHP BK- and M-currents. To study the apamin-sensitive currents in relative isolation, the I_{sAHP} BK current and M-current were suppressed by including 100 μM cAMP (cAMP or 8CPT-cAMP) in the intracellular medium of the recording pipette and 5 mM TEA plus 10 μM XE991 in the extracellular medium throughout each experiment. Tail currents from representative CA1 (*A*) and CA3 (*B*) pyramidal cells and a DG granule cell (*C*) are shown. The currents were elicited and recorded using the same voltage-clamp protocol as in Figure 5 (holding potential, –55 mV; 100 msec step). For each cell (*A–C*), records before (*Control*) and after application of 100 nM apamin are shown. Note that the DG granule cells showed no net outward tail current under these conditions. Furthermore, the apamin-sensitive current isolated by digital subtraction (*Subtracted*) was far smaller in the DG neurons than in the CA1 and CA3 neurons and decayed more slowly in CA3 than in CA1 cells. *Superimposed*, Comparison of the records before and after apamin application. *D, E*, Comparison between typical time courses of the effect of apamin (100 nM) application (*gray bar*) on the early tail current (normalized; control = 100%) in a pyramidal cell (*D*) and a DG granule cell (*E*). The apamin effects in CA1 and CA3 pyramidal cells were similar (the example shown in *D* is from a CA3 cell), whereas the effect was much weaker in DG cells. Note in both cell types the slight time-dependent run-down of the currents. In pyramidal cells, an initial increase ("run-up") of the current amplitude was sometimes observed (*D*; 0–3 min). *F, G*, Summary data comparing apamin-sensitive currents (*F*) and current densities (*G*) in CA1 pyramidal cells ($n = 9$), CA3 pyramidal cells ($n = 8$), and DG granule cells ($n = 7$). *D*, Peak amplitudes of the apamin-sensitive tail current obtained by subtraction of records before and after application of 100 nM apamin. *G*, Current densities obtained by dividing the measurements shown in *F* by the whole-cell capacitance measured in each cell.

SK1 gene (but not the SK2 and SK3 genes) undergoes extensive alternative splicing. Mouse and rat brain express at least eight 3′-variant SK1 transcripts with additional heterogeneity in the 5′ region (Shmukler et al., 2001). To obtain a clear picture of the distribution of the entire SK1 channel population, N- and C-terminal SK1 antibodies were used. In immunoblotting experiments the N-terminal antibody revealed the tissue expression of three SK1 polypeptide families with apparent M_r values of 65, 58, and 43 kDa, respectively (Fig. 1). The reported cDNA sequences also subdivided the putative SK1 polypeptides into three distinct groups with predicted M_r values of 62, 57–58, and 45–49 kDa. A C-terminal anti-SK1 antibody detected only polypeptides with apparent M_r values of 65 and 58 kDa, respectively. These results are in agreement with the alternative splicing data (the truncated SK1 polypeptides are expected to lack the respective antibody recognition sequences). Remarkably, we did not obtain any evidence for alternative splicing at the N terminus. In contrast to SK1 protein, the anti-SK2 and anti-SK3 antibodies labeled only single polypeptides with apparent M_r values of 67 and 70 kDa, respectively.

After having established that our antibodies specifically recognize their respective target proteins, we used them to establish the distribution of all known SK channels. The three SK channel subunits displayed distinct although sometimes overlapping distribution. Most of the higher brain regions such as the neocortex and hippocampus showed expression of both SK1 and SK2 channels, whereas phylogenetically older brain regions (e.g., the thalamus, basal ganglia, cerebellum, and brainstem) showed high levels of SK3 expression. The strong expression of SK3 channel protein in the basal ganglia and brainstem was also previously observed for the mouse brain (Bond et al., 2000).

A particular informative distribution pattern was observed for the hippocampal formation. High levels of SK2 expression in the CA1–CA3 fields contrasted with the low levels in the dentate gyrus. Conversely, for SK1 protein, high levels were detected in the DG with lower levels in CA1–CA3. Immunoreactivity for these SK proteins was found in regions containing densely packed dendrites of pyramidal cells (SK1- and SK2-IR) or DG granule cells (SK1-IR). Considering that the granule cells are more numerous and smaller, with thinner dendritic shafts, than the pyramidal cells (Amaral et al., 1990), there may be more neuronal plasma membrane area per volume unit in the DG than in CA1–CA3. If so, the relatively weak SK2 staining in the DG may reflect a still lower density of SK2 protein per membrane area relative to CA1–CA3. Conversely, the stronger SK1 staining in the DG relative to CA1–CA3 may not necessarily represent a higher density of SK1 protein per membrane area.

SK3 protein in rat hippocampus is expressed only at moderate to low levels (Figs. 3, 4) with the most prominent staining observed in the mossy fiber system. This distribution in conjunction with the characteristic immunostaining of varicose fibers throughout the hippocampal formation suggests most likely an axonal or presynaptic localization of SK3 protein. This proposed subcellular targeting is supported by recent colocalization studies in cultured neonatal hippocampal neurons in which SK3 protein clearly coresides with established presynaptic marker proteins (e.g., synapsin; Obermair et al., 2001).

On the basis of the distinct distribution pattern in the hippocampal formation, this brain region was chosen for functional investigations. Whole-cell patch-clamp recordings revealed a striking difference in the functional expression of the apamin-sensitive outward current I_{aAHP} between the DG granule cells

Table 2. Cells recorded with cAMP in the pipette (I_{sAHP} suppressed)

	Apamin-sensitive current, I_{aAHP}			
	Amplitude (pA)[a]	Decay time constant (msec)[a]	Current density (A/F)[a]	*n*
CA1	130.0 ± 18.1	177.2 ± 30.1	0.80 ± 0.10	9
CA3	152.5 ± 23.8	297.0 ± 23.0	0.75 ± 0.10	8
DG	29.6 ± 4.4	[b]	0.38 ± 0.06	7

[a]Values are mean ± SEM.

[b]The amplitude of the current in DG cells was too small to reliably determine the decay time constant.

Table 3. *p* values from statistical comparisons (two-tailed paired Student's *t* test)

Condition	CA1 versus CA3	DG versus CA1	DG versus CA3
No cAMP			
I_{aAHP} amplitude	0.0063	0.0070	0.00006
I_{aAHP} decay time constant	0.082		
I_{aAHP} density	0.067	0.0057	0.00011
I_{sAHP} density	0.18	0.45	0.089
With cAMP in the pipette			
I_{aAHP} amplitude	0.46	0.00045	0.0012
I_{aAHP} decay time constant	0.0082		
I_{aAHP} density	0.62	0.0049	0.012

and the CA1–CA3 pyramidal cells. Whereas the pyramidal cells showed a robust I_{aAHP} of ~100 pA (80–130 pA in CA1 and 120–150 pA in CA3), I_{aAHP} was an order of magnitude smaller in the granule cells (~8 pA under normal conditions) (Figs. 5, 6, Table 1). Even when corrected for the membrane capacitance of the cells (which is approximately proportional to their surface area), the currents (i.e., current densities) were still approximately twice as high in CA1–CA3 as in DG (~0.8 pA/pF in CA1–CA3 vs 0.4 pA/pF in DG). In contrast, the average density of the slow AHP current was somewhat larger in the DG than in CA1–CA3.

The apamin-sensitive SK current (~30 pA) detected in DG granule cells was significantly enhanced when the cells were perfused with cAMP analogues and other outward currents were suppressed ($p = 0.002$). This difference and the increased mean I_{aAHP} in the pyramidal cells treated with cAMP may reflect a cAMP-induced upregulation of SK channels (as suggested for CA1 cells; Stocker et al., 1999). However, the difference in the observed I_{aAHP} amplitude between CA1–CA3 and the DG cannot be explained by different cAMP regulation of the SK channels in the two regions, because the contrast was observed either with or without cAMP in the pipette. In addition to cAMP effects, improved clamp conditions may contribute to the larger SK currents observed during blockade of other K^+ currents. The difference in SK current is probably not attributable to a difference in Ca^{2+} influx between CA1–CA3 and DG cells, because the Ca^{2+} currents were stable throughout the recordings and elicited robust sAHP currents of similar amplitude in all three cell types (Figs. 5, 6, Tables 1–3).

There seems to be a close agreement between the functional expression of apamin-sensitive current and the distribution of SK2 protein in the hippocampal principal neurons. Thus, the SK2 protein levels, as well as the apamin-sensitive current amplitudes, were highest in CA1–CA3 and substantially lower in the DG. In contrast, the differences in currents do not match the SK3 protein distribution, which was rather uniform throughout the entire hippocampal formation. This suggests that SK2 underlies the apamin-sensitive mAHP component of the CA1 and CA3 pyramidal cells. Because only SK2 homomultimers were detected by coimmunoprecipitation (Fig. 2*B,C*), it is likely that this channel type underlies the apamin-sensitive mAHP and, hence, the apamin-sensitive early spike frequency adaptation in the hippocampal pyramidal cells. However, it remains to be determined whether SK1 protein contributes to the apamin-sensitive AHP in the DG granule cells, where this SK species is more strongly expressed.

Why does the decay time course of the apamin-sensitive current differ between CA1 and CA3 pyramidal cells? This seems to most simply be explained by different Ca^{2+} dynamics, subcellular distribution of SK2 channels, or both, between the two cell types. The time course of the SK2 and SK3 channel activity is known to closely follow the rise in intracellular Ca^{2+} (Vergara et al., 1998). The SK channels open and close rapidly in response to changes in intracellular $[Ca^{2+}]$ and show little or no intrinsic time dependence at the time scale relevant for the overall tail current kinetics. Thus, the SK current time course probably reflects the Ca^{2+} dynamics of the particular cell type and subcellular domain where the channels are located, independently of the SK channel subtype involved. Therefore, the difference in time course between CA1 and CA3 seems fully compatible with the hypothesis that SK2 homomultimers generate the apamin-sensitive mAHP in both cell types.

The relatively large sAHP current density in DG granule cells compared with CA1–CA3 pyramidal cells seems to approximately parallel the high levels of SK1 protein in the DG relative to CA1–CA3. This, along with the lower apamin sensitivity of homomeric SK channels, may seem to support the hypothesis that SK1 underlies the apamin-insensitive sAHP. However, this idea seems still difficult to reconcile with the observation that the hippocampal sAHP seems to be entirely resistant to high concentrations of apamin, which completely block the homomultimeric SK1 channels tested in different expression systems (Shah and Haylett, 2000a; Strobaek et al., 2000; Grunnet et al., 2001b). This hypothesis might, however, be rescued if there exist auxiliary (β) subunits that substantially alter the toxin sensitivity of the SK channel complex, such as the BK-β4 subunits have been found to do for BK channels (Meera et al., 2000).

REFERENCES

Amaral DG, Ishizuka N, Claiborne B (1990) Neurons, numbers and the hippocampal network. Prog Brain Res 83:1–11.

Bond CT, Sprengel R, Bissonette JM, Kaufmann WA, Pribnoff D, Neelands T, Storck T, Baetscher M, Jerecic J, Knaus HG, Seeburg PH, Adelman JP (2000) Respiration and parturition affected by conditional overexpression of the small conductance Ca^{2+}-activated K^+ channel subunit, SK3. Science 289:1942–1946.

Bowden SE, Fletcher S, Loane DJ, Marrion NV (2001) Somatic colocalization of rat SK1 and D class [Ca(v)1.2] L-type calcium channels in rat CA1 hippocampal pyramidal neurons. J Neurosci 21:RC175:1–6.
Faber ES, Sah P (2002) Physiological role of calcium-activated potassium currents in the rat lateral amygdala. J Neurosci 22:1618–1628.
Grunnet M, Jensen BS, Olesen SP, Klaerke DA (2001a) Apamin interacts with all subtypes of cloned small-conductance Ca^{2+}-activated K^+ channels. Pflügers Arch 441:544–550.
Grunnet M, Jespersen T, Angelo K, Frokjaer-Jensen C, Klaerke DA, Olesen SP, Jensen BS (2001b) Pharmacological modulation of SK3 channels. Neuropharmacology 40:879–887.
Haas HL, Rose GM (1987) Noradrenaline blocks potassium conductance in rat dentate granule cells in vitro. Neurosci Lett 78:171–174.
Hirschberg B, Maylie J, Adelman JP, Marrion NV (1998) Gating of recombinant small-conductance Ca-activated K^+ channels by calcium. J Gen Physiol 111:565–581.
Hotson JR, Prince DA (1980) A calcium-activated hyperpolarization follows repetitive firing in hippocampal neurons. J Neurophysiol 43:409–419.
Hu H, Shao LR, Chavoshy S, Gu N, Trieb M, Behrens R, Laake P, Pongs O, Knaus HG, Ottersen OP, Storm JF (2001) Presynaptic Ca^{2+}-activated K^+ channels in glutamatergic hippocampal terminals and their role in spike repolarization and regulation of transmitter release. J Neurosci 21:9585–9597.
Ishii TM, Maylie J, Adelman JP (1997) Determinants of apamin and d-tubocurarine block in SK potassium channels. J Biol Chem 272:23195–23200.
Keen JE, Khawaled R, Farrens DL, Neelands T, Rivard A, Bond CT, Janowsky A, Fakler B, Adelman JP, Maylie J (1999) Domains responsible for constitutive and Ca^{2+}-dependent interactions between calmodulin and small conductance Ca^{2+}-activated potassium channels. J Neurosci 19:8830–8838.
Knaus HG, Eberhart A, Koch RO, Munujos P, Schmalhofer WA, Warmke JW, Kaczorowski GJ, Garcia ML (1995) Characterization of tissue-expressed alpha subunits of the high conductance Ca^{2+}-activated K^+ channel. J Biol Chem 270:22434–22439.
Knaus HG, Schwarzer C, Koch RO, Eberhart A, Kaczorowski GJ, Glossmann H, Wunder F, Pongs O, Garcia ML, Sperk G (1996) Distribution of high-conductance Ca^{2+}-activated K^+ channels in rat brain: targeting to axons and nerve terminals. J Neurosci 16:955–963.
Kohler M, Hirschberg B, Bond CT, Kinzie JM, Marrion NV, Maylie J, Adelman JP (1996) Small-conductance, calcium-activated potassium channels from mammalian brain. Science 273:1709–1714.
Koschak A, Koch RO, Liu J, Kaczorowski GJ, Reinhart PH, Garcia ML, Knaus HG (1997) [125I]Iberiotoxin-D19Y/Y36F, the first selective, high specific activity radioligand for high-conductance calcium-activated potassium channels. Biochemistry 36:1943–1952.
Koschak A, Bugianesi RM, Mitterdorfer J, Kaczorowski GJ, Garcia ML, Knaus HG (1998) Subunit composition of brain voltage-gated potassium channels determined by hongotoxin-1, a novel peptide derived from *Centruroides limbatus* venom. J Biol Chem 273:2639–2644.
Lai JC, Walsh JM, Dennis SC, Clark JB (1977) Synaptic and nonsynaptic mitochondria from rat brain: isolation and characterization. J Neurochem 28:625–631.
Lancaster B, Adams PR (1986) Calcium-dependent current generating the afterhyperpolarization of hippocampal neurons. J Neurophysiol 55:1268–1282.
Lancaster B, Nicoll RA (1987) Properties of two calcium-activated hyperpolarizations in rat hippocampal neurones. J Physiol (Lond) 389:187–203.
Madison DV, Nicoll RA (1986) Cyclic adenosine 3′,5′-monophosphate mediates beta-receptor actions of noradrenaline in rat hippocampal pyramidal cells. J Physiol (Lond) 372:245–259.
Meera P, Wallner M, Toro L (2000) A neuronal beta subunit (KCNMB4) makes the large conductance, voltage- and Ca^{2+}-activated K^+ channel resistant to charybdotoxin and iberiotoxin. Proc Natl Acad Sci USA 97:5562–5567.
Obermair GJ, Pragl B, Knaus HG, Flucher BE (2001) Presynaptic localisation of Ca^{2+}-activated K^+ channel SK3 in cultured mouse hippocampal neurons. Biophys J 80 [Suppl 1]:234a.
Partridge LD, Swandulla D (1993) Control of cell function by neuronal calcium-activated nonselective (CAN) cation channels. EXS 66:175–183.
Pedarzani P, Storm JF (1993) PKA mediates the effects of monoamine transmitters on the K^+ current underlying the slow spike frequency adaptation in hippocampal neurons. Neuron [Erratum (1994) 12:934] 11:1023–1035.
Pennefather P, Lancaster B, Adams PR, Nicoll RA (1985) Two distinct Ca^{2+}-dependent K^+ currents in bullfrog sympathetic ganglion cells. Proc Natl Acad Sci USA 82:3040–3044.
Sah P (1996) Ca^{2+}-activated K^+ currents in neurones: types, physiological roles and modulation. Trends Neurosci 19:150–154.
Shah M, Haylett DG (2000a) The pharmacology of hSK1 Ca^{2+}-activated K^+ channels expressed in mammalian cell lines. Br J Pharmacol 129:627–630.
Shah M, Haylett DG (2000b) Ca^{2+} channels involved in the generation of the slow afterhyperpolarization in cultured rat hippocampal pyramidal neurons. J Neurophysiol 83:2554–2561.
Shah MM, Miscony Z, Javadzadeh-Tabatabaie M, Ganellin CR, Haylett DG (2001) Clotrimazole analogues: effective blockers of the slow afterhyperpolarization in cultured rat hippocampal pyramidal neurones. Br J Pharmacol 132:889–898.
Shmukler BE, Bond CT, Wilhelm S, Bruening-Wright A, Maylie J, Adelman JP, Alper SL (2001) Structure and complex transcription pattern of the mouse SK1 K(Ca) channel gene, KCNN1. Biochim Biophys Acta 1518:36–46.
Stocker M, Pedarzani P (2000) Differential distribution of three Ca^{2+}-activated K^+ channel subunits, SK1, SK2, and SK3, in the adult rat central nervous system. Mol Cell Neurosci 15:476–493.
Stocker M, Krause M, Pedarzani P (1999) An apamin-sensitive Ca^{2+}-activated K^+ current in hippocampal pyramidal neurons. Proc Natl Acad Sci USA 96:4662–4667.
Storm JF (1987) Action potential repolarization and a fast after-hyperpolarization in rat hippocampal pyramidal cells. J Physiol (Lond) 385:733–759.
Storm JF (1989) An after-hyperpolarization of medium duration in rat hippocampal pyramidal cells. J Physiol (Lond) 409:171–190.
Storm JF (1990) Potassium currents in hippocampal pyramidal cells. Prog Brain Res 83:161–187.
Strobaek D, Jorgensen TD, Christophersen P, Ahring PK, Olesen SP (2000) Pharmacological characterization of small-conductance Ca^{2+}-activated K^+ channels stably expressed in HEK 293 cells. Br J Pharmacol 129:991–999.
Tacconi S, Carletti R, Bunnemann B, Plumpton C, Merlo PE, Terstappen GC (2001) Distribution of the messenger RNA for the small conductance calcium-activated potassium channel SK3 in the adult rat brain and correlation with immunoreactivity. Neuroscience 102:209–215.
Vazquez J, Feigenbaum P, King VF, Kaczorowski GJ, Garcia ML (1990) Characterization of high affinity binding sites for charybdotoxin in synaptic plasma membranes from rat brain: evidence for a direct association with an inactivating, voltage-dependent, potassium channel. J Biol Chem 265:15564–15571.
Vergara C, Latorre R, Marrion NV, Adelman JP (1998) Calcium-activated potassium channels. Curr Opin Neurobiol 8:321–329.
Wang GY, Robinson DW, Chalupa LM (1998) Calcium-activated potassium conductances in retinal ganglion cells of the ferret. J Neurophysiol 79:151–158.
Williamson A, Alger BE (1990) Characterization of an early afterhyperpolarization after a brief train of action potentials in rat hippocampal neurons in vitro. J Neurophysiol 63:72–81.
Wouterlood FG (1988) Anterograde neuroanatomical tracing with *Phaseolus vulgaris*-leucoagglutinin combined with immunocytochemistry of gamma-aminobutyric acid, choline acetyltransferase or serotonin. Histochemistry 89:421–428.
Xia XM, Fakler B, Rivard A, Wayman G, Johnson-Pais T, Keen JE, Ishii T, Hirschberg B, Bond CT, Lutsenko S, Maylie J, Adelman JP (1998) Mechanism of calcium gating in small-conductance calcium-activated potassium channels. Nature 395:503–507.